$^3He(\vec{t}, t)^3He$ elastic scattering measurements from 9 to 17 MeV

R. F. Haglund, Jr., G. G. Ohlsen, R. A. Hardekopf, Nelson Jarmie, Ronald E. Brown,* and P. A. Schmelzbach†

Los Alamos Scientific Laboratory, University of California,‡ Los Alamos, New Mexico 87545

(Received 20 December 1976)

Angular distributions of the analyzing power and differential cross section for $^3He(\vec{t}, t)^3He$ elastic scattering are reported for triton bombarding energies of 9.02, 11.00, 13.02, 15.02, 16.00, and 17.02 MeV, over a c.m. angular range from 25° to 155°. Excitation functions for the analyzing power are presented for the energy range 14.42–17.22 MeV. Problems in the phase-shift analysis of the data are discussed.

[NUCLEAR REACTIONS $^3He(\vec{t}, t)$, E_t = 9.02, 11.00, 13.02, 15.02, 16.00, 17.02 MeV. Measured $A_y(\theta)$, θ = 25°–155°; $A_y(E)$, E = 14.42–17.22 MeV; $\sigma(\theta)$, θ = 30°–150°.]

I. INTRODUCTION

The most extensively studied six-nucleon system is ^6Li (Ref. 1), which can be formed in two different ways using charged-particle reactions: with deuterons plus ^4He or tritons plus ^3He. In either case, information on both cross sections and spin-dependent observables is necessary for an adequate analysis.

Previous theoretical treatments include resonating-group calculations,[2,3] cluster-model treatments,[4] and extensive phase-shift analyses.[5] However, the polarization data used in these analyses have come from ^4He-d elastic scattering experiments which cover a range of relatively low excitation energies in the compound system ^6Li (4–13 MeV).

The recent installation of a polarized-^3He source[6] at the University of Birmingham and of a polarized-triton source[7] at the Los Alamos Scientific Laboratory has made it possible to obtain extensive polarization data on the six-nucleon system through $^3He + \vec{t}$ and $^3H + {}^3\vec{He}$ elastic scattering. Such measurements are easily carried out because of the spin-$\frac{1}{2}$ character of the projectiles. Also, because the $^3He + t$ threshold lies at 15.8-MeV excitation energy in ^6Li, a new range of excitation energies can be studied in such experiments.

In this paper, we present analyzing power and cross section angular distributions extracted from $^3He(\vec{t}, t)^3He$ elastic scattering at triton energies between 9 and 17 MeV, and a limited set of analyzing-power excitation functions. The cross sections are found to give generally good agreement with other measurements in this energy range.[8,9] Finally, we discuss appropriate methods for the analysis of these data.

II. EXPERIMENTAL PROCEDURE

Our measurements were made using the LASL polarized-triton source and FN tandem Van de Graaff accelerator. The beam from the accelerator was incident on a 9.7-cm-diam gas cell, with a 300° exit foil window (Fig. 1). The entrance foil window was of 2.5-μm Havar foil,[10] while the exit foil was 2.5-μm Havar foil for some of the angular distributions (at 9, 13, 15, and 17 MeV) and 6.3-μm Kapton[10] for the others (at 11 and 16 MeV). The snout of the gas cell contained a 2.5-mm-diam entrance collimator, and two antiscattering slits of slightly larger diameters.[11] Further details of the beam optics may be found in Ref. 11. The nominal pressure in the cell was 300 Torr; this pressure was recorded and the cell refilled periodically. The pressure variation during any given measurement at one angle was less than 1%. Pressure variations between readings were assumed to be linear. For the measurements at 11 and 16 MeV, a 0.3-liter buffer tank was attached to the gas cell, to reduce pressure losses from the diffusion of ^3He through the Kapton. To minimize the consumption of ^3He, the cell was filled and emptied from a recirculating pump system.

Counter telescopes containing two or three silicon surface-barrier detectors were mounted on

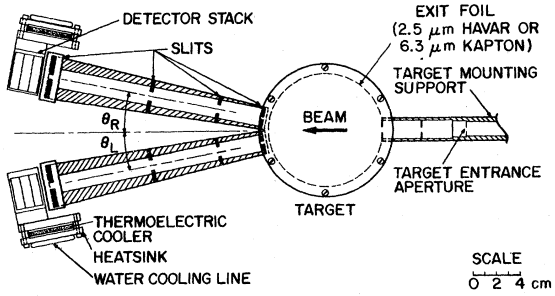

FIG. 1. Schematic diagram of the gas target and detectors. The entrance tube of the target and the detector collimator snouts are presented in cut-away view to show the location of the beam- and solid-angle-defining slits.

the "left" and "right" turntables of a 60-cm cubical scattering chamber,[11,12] known locally as the "Supercube." The turntable position—and hence the lab scattering angle—was controlled by an SDS-930 on-line computer, using optical shaft encoders to provide a position signal. The scattering angle could be set by this method to ±0.02° (Ref. 11), which gives a relative accuracy of ±0.05° for angles in the c.m. system. The zero of the left and right turntables is known to ±0.05°. Hence, the scale error for angles in the c.m. system is ±0.1°.

The slit system for the telescopes consisted of a front slit, two antiscatter slits and a rear slit, as shown in Fig. 1. The front and rear slits were 3.3 mm wide, corresponding to an angular acceptance of 1° full width at half maximum (FWHM). For measurements made with two-detector telescopes (at 9, 13, 15, and 17 MeV) the rear slit height was 11.4 mm. For measurements made with three-detector telescopes (at 11 and 16 MeV), the rear slit height was reduced to 6.25 mm to ensure that there would be no multiple-scattering losses in the detector stack. The rear slit was located 24.1 cm from the center of the gas cell, and the separation between front and rear slits was 19.0 cm. This gave a nominal detector geometry factor G_{00} (see Ref. 13) of 2.76×10^{-4} (1.51×10^{-4}) cm sr for the taller (shorter) rear slits.

The average current delivered to the target was about 50 nA. The beam polarization varied slowly over a range from 0.71 to 0.78 during the experiments, but remained constant to within ±0.02 during the data-taking sequence for individual points. The beam polarization was measured by the quench-ratio method.[14] The position of the beam was monitored by two sets of four-way slits. The first set was located at the entrance of the scattering chamber, 60 cm ahead of the target center. The second set of slits was built into the electrically suppressed Faraday cup assembly, 66 cm behind the center of the gas cell. By adjusting the currents on these two sets of slits, the beam could be centered horizontally and vertically in the target. The currents on the second set of slits and on the beam stop just behind them were summed to give the total beam current.

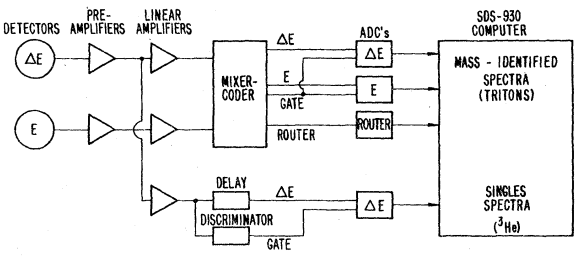

FIG. 2. Block diagram of electronics used with a two-detector telescope (right or left arm only).

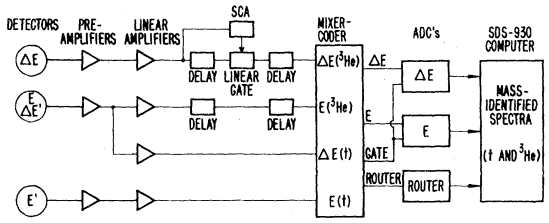

FIG. 3. Block diagram of electronics used with a three-detector telescope (right or left arm only).

The measurements at 9, 13, 15, and 17 MeV were made with two-detector counter telescopes consisting of 150-μm ΔE surface-barrier detectors (50 μm for the 9-MeV measurements) and 1000-μm E detectors. Signals from the detectors were preamplified in two stages, and processed as shown in Fig. 2. Both the ΔE and E pulses were sent to a mixer-coder,[15] which tags coincident ΔE-E signals with a routing pulse and forwards them through analog-to-digital converters (ADC's) to the on-line computer. Mass identification was accomplished on-line in the computer, following the procedure detailed in Ref. 15.

For the measurements with two-detector telescopes, separate ADC's were used to store simultaneously the ΔE *singles* spectrum, in which the ^{3}He particles could be identified by their energy loss. The background in these singles spectra was always higher than for the mass-identified triton spectra. Some of the triton data at 9 MeV were also acquired in singles mode.

At beam energies of 11 and 16 MeV, the data were acquired using three-detector counter telescopes. Each of these consisted of two fully depleted ΔE detectors and a partially depleted E detector. At 11 MeV, the nominal thicknesses were 17, 75, and 300 μm, and at 16 MeV, the detectors were 40, 150, and 1000 μm thick. These thicknesses were chosen in such a way that both ^{3}He particles and tritons could be mass-identified, the the former in the front pair of detectors and the latter in the rear pair. The electronics for this scheme is shown in Fig. 3. In general, the energy loss for the tritons in the first ΔE detector was less than the threshold of the mixer-coder. When this was not the case, the lower-level discriminator of the single-channel analyzer in the ^{3}He ΔE circuit was set just high enough to cut off the triton signals, thereby reducing dead time to a minimum.

Both triton and ^{3}He spectra were displayed individually for each counter telescope on an oscillo-

scope screen. Foreground and background gates were set separately for each spectrum, and the selected peaks were integrated by the on-line computer, either with or without linear background subtraction.

For each energy and angle, the data were taken as follows. The counter telescopes were set at equal angles left and right of the incident beam direction. With the spin quantization axis in the up direction (perpendicular to the reaction plane) counts in the left and right detectors were recorded for a preset amount of integrated charge. The spin quantization axis was then reversed in the polarized-triton source, so that the spin was down at the target, and the procedure repeated. The beam polarization was measured before and after each spin-up and each spin-down run, and the result was stored in the on-line computer.

The geometric means of the integrated peak sums

$$L = [\text{left, spin up})\,(\text{right, spin down})]^{1/2}$$

and

$$R = [(\text{right, spin up})\,(\text{left, spin down})]^{1/2}$$

were then computed.[16] In terms of these quantities, the vector analyzing power is[17]

$$A_y = \frac{1}{p}\frac{L-R}{L+R}, \tag{1}$$

where p is the average beam polarization. This data collection scheme eliminates all first-order errors in A_y associated with instrumental asymmetries and alignment errors.[17]

The lab differential cross section σ_0 is proportional to the yield

$$Y = \tfrac{1}{2}(L+R). \tag{2}$$

For the cross section measurement, the use of symmetric geometry is advantageous because it compensates for angular errors due to beam wander during data taking.

The estimated uncertainties in the quoted beam energies include a scale error arising from the absolute calibration of the beam analyzing magnet, and relative errors stemming from nonlinearity of the analyzing magnet and uncertainties in the calculated beam energy losses in the target.

The tandem Van de Graaff energy calibration is based on a measurement of the ^{12}C(p,p)^{12}C isospin-forbidden resonance at 14.230 75 ± 0.000 20 MeV.[18] We believe the scale error in the calibration of the analyzing magnet from this measurement to be not more than ±1 keV. The relative calibration errors arising from nonlinearities in the analyzing magnet and from magnet-recycling and slit-setting procedures have not been studied. However, we estimate this error to be at most ±3 keV. The uncertainty in the energy-loss calculations for tritons entering the gas cell is about ±2 keV. The uncertainty in the thickness of the Havar entrance foil on the gas cell contributes an additional relative error of ±11 keV. A quadratic sum of all these relative errors gives an overall energy uncertainty of ±12 keV.

The energy spread of the incident beam at the target is dominated by straggling in the Havar entrance foil and the target gas in the cell. Calculations with the code STRAGL[19] give mean straggling widths of 29 keV in the Havar foil and 16 keV in the ^{3}He target gas. The variation in these values is less than ±1 keV over the triton energy range 9–17 MeV. (Bohr's energy-independent approximate formula[20] gives straggling widths of 29 keV in the Havar foil and 17 keV in the ^{3}He gas.) When the Havar and gas straggling widths are folded quadratically with the estimated ±4-keV terminal ripple of the Van de Graaff, the total energy spread in the incident beam is calculated to be 33 keV FWHM.

III. RESULTS AND ERROR ANALYSIS

A. Analyzing power

Angular distributions of the analyzing power A_y were measured at triton lab energies of 9.02, 11.00, 13.02, 15.02, 16.00, and 17.02 meV. Both triton and ^{3}He recoil groups were recorded at intervals of 2.5° from 12.5° to 45° (lab). This produced angular distributions in 5° steps from 25° to 155° in the center-of-mass system, since

$$A_y(\theta)_{\text{triton}} = -A_y(\pi-\theta)_{^3\text{He}}. \tag{3}$$

The point at $\theta_{\text{lab}} = 45°$ gave a consistency check, since the scattered tritons and recoil ^{3}He particles both correspond to 90° c.m. angle. Additional overlap points were taken where possible.

The angular distributions are displayed in Figs. 4 and 5 with triton data shown as dots and ^{3}He data as triangles. The errors in the recoil ^{3}He data include the background error in the singles ΔE spectra from which the ^{3}He peak sums were extracted. The background in the triton spectra was always very small. Numerical values for A_y are presented in Table I.

Between 15 and 17 MeV, the angular distribution changes shape. To elucidate this change, we measured excitation functions from 14.42 to 17.22 MeV at lab angles of 22.5° and 37.5°. By measuring both tritons and ^{3}He recoil particles at these angles, we obtained excitation functions for four c.m. angles. These data (see Fig. 6 and Table II) show only gradual trends upward or downward, although the 75° excitation function shows a much

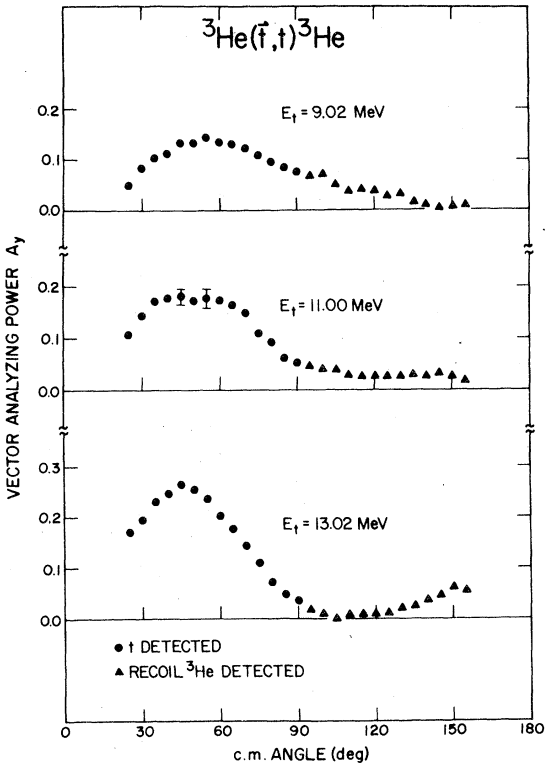

FIG. 4. Angular distributions of the analyzing power for ^{3}He +$\vec{t}$ elastic scattering at triton lab energies of 9.02, 11.00, and 13.02 MeV. Only relative errors are shown. Where no error bars appear, the relative errors are smaller than the plotting symbols.

steeper slope than the others.

The relative errors in A_y arise from the following: (1) statistical errors in the peaks, including the error due to background subtraction; (2) random errors in setting the background gates under the peaks of interest; (3) random errors in the measurement of the beam polarization by the quench-ratio method; and (4) random systematic errors, such as position instability in the beam. The errors shown in Tables I and II are *relative* errors, and are obtained by quadratically combining the contributions of (1), (2), and (3) together with 0.005, which we believe to be a reasonable estimate of the errors due to (4). This value for the random systematic error is based on experience with repeatability of data for this type of experiment.

The normalization or scale error for A_y arises solely from errors in determining the absolute value of the beam polarization using the quench-ratio technique, since all other scale errors cancel for data taken with symmetric geometry.[17] The sources of scale error include the following: (1) the presence of an unpolarized, negatively-charged background in the incident beam—which masquerades as polarized beam when electric, rather than magnetic, fields are used for quenching[14]; (2) enhancement of the polarization by slit-edge scraping as the beam goes from the analyzing-magnet Faraday cup (where the quench ratio is measured) to the target[14,21]; (3) the small, negative polarization in the *quenched* beam[14]; and (4) depolarization due to residual gas in the terminal of the tandem Van de Graaff.[22]

The effect of (1) can be checked periodically during the course of an experiment. We found the discrepancies between electric- and magnetic-field quench ratios to be typically 0.010–0.015 with infrequent excursions to as much as 0.025. Polari-

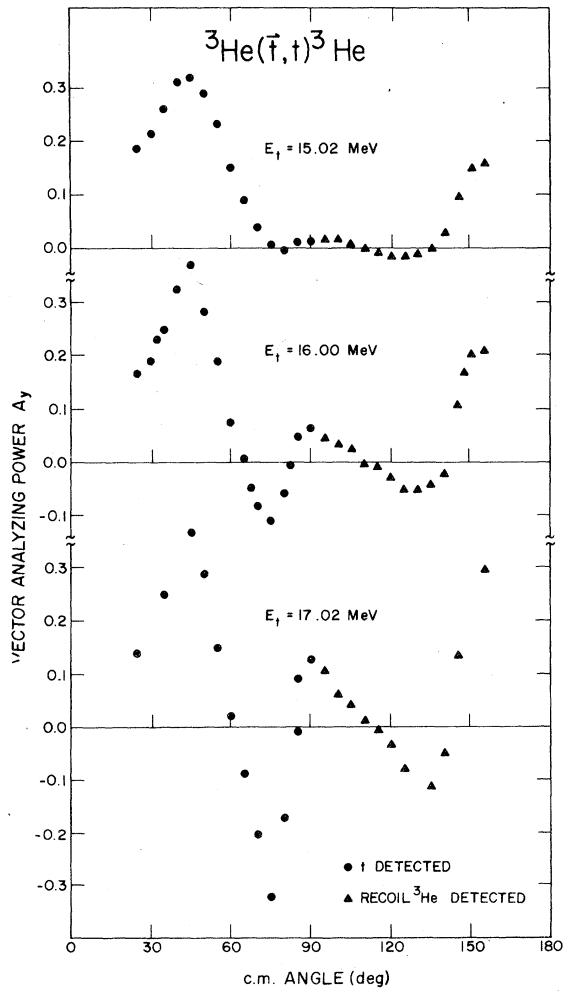

FIG. 5. Angular distributions of the analyzing power for ^{3}He +$\vec{t}$ elastic scattering at triton lab energies of 15.02, 16.00, and 17.02 MeV. The relative errors are smaller than the plotting symbols.

TABLE I. Analyzing power angular distributions $A_y(\theta)$ for ^{3}He($\vec{t}$,t)^{3}He at the stated energies. Relative errors ΔA_y are indicated in the table. Scale error is ± 0.02 times A_y.

c.m. angle (deg)	Triton lab energy 9.02 MeV		11.00 MeV		13.02 MeV		15.02 MeV		16.00 MeV		17.02 MeV	
	A_y	ΔA_y	A_y	ΔA_y	A_y	ΔA_y	A_y	ΔA_y	A_y	ΔA_y	A_y	ΔA_y
25.05	0.048	0.007	0.108	0.007	0.170	0.007	0.186	0.006	0.165	0.009	0.139	0.006
30.05	0.083	0.008	0.144	0.009	0.193	0.011	0.214	0.006	0.189	0.009	0.176	0.006
32.55	...	...	...	...	...	...	...	...	0.230	0.009	...	...
35.05	0.103	0.009	0.178	0.009	0.230	0.008	0.260	0.008	0.245	0.009	0.247	0.007
40.05	0.110	0.009	0.177	0.009	0.245	0.006	0.310	0.006	0.324	0.011	0.337	0.008
45.05	0.133	0.007	0.181	0.020	0.262	0.006	0.319	0.008	0.368	0.014	0.367	0.008
50.05	0.131	0.007	0.173	0.009	0.252	0.006	0.290	0.007	0.281	0.014	0.287	0.008
55.05	0.142	0.011	0.179	0.017	0.235	0.006	0.232	0.007	0.188	0.015	0.149	0.009[a]
60.05	0.134	0.007	0.173	0.009	0.200	0.007	0.151	0.006	0.074	0.016[a]	0.019	0.007[a]
65.05	0.131	0.011	0.165	0.009	0.174	0.007	0.090	0.006[a]	0.006	0.013[a]	−0.088	0.007[a]
67.55	...	...	...	...	...	...	...	...	−0.049	0.015[a]	...	...
70.05	0.121	0.009	0.147	0.009	0.142	0.006	0.037	0.006[a]	−0.085	0.016[a]	−0.205	0.007[a]
75.05	0.107	0.007	0.107	0.010	0.108	0.006	0.007	0.007[a]	−0.112	0.019[a]	−0.324	0.008[a]
80.05	0.094	0.007	0.092	0.010	0.071	0.007	−0.005	0.007[a]	−0.060	0.020[a]	−0.171	0.009[a]
82.55	...	...	...	...	...	...	...	...	−0.008	0.025[a]	...	...
85.05	0.084	0.007	0.061	0.010	0.048	0.009[a]	0.013	0.007[a]	0.047	0.017[a]	0.091	0.011[a]
90.05	0.075	0.019	0.053	0.010	0.035	0.009[a]	0.014	0.006[a]	0.063	0.021[a]	0.127	0.007[a]
94.95	0.068	0.014	0.048	0.011	0.019	0.007	0.017	0.005[b]	0.045	0.011[b]	0.107	0.006[b]
97.45	...	...	...	...	...	...	...	...	0.038	0.012[b]	...	...
99.95	0.070	0.012	0.041	0.009	0.011	0.006	0.018	0.005[b]	0.032	0.009[b]	0.064	0.005[b]
104.95	0.050	0.010	0.040	0.009	0.002	0.009	0.009	0.005	0.025	0.009[b]	0.043	0.005[b]
109.95	0.037	0.013	0.029	0.009	0.010	0.005	0.001	0.005	−0.004	0.008	0.012	0.005[b]
112.45	...	...	...	...	...	...	...	...	−0.004	0.008	...	...
114.95	0.041	0.013	0.029	0.009	0.010	0.006	−0.007	0.005	−0.009	0.007	−0.006	0.005[b]
119.95	0.039	0.013	0.026	0.009	0.010	0.006	−0.014	0.005	−0.030	0.009	−0.034	0.005[b]
124.95	0.028	0.013	0.026	0.009	0.013	0.005	−0.011	0.006	−0.047	0.009	−0.076	0.006
129.95	0.031	0.011	0.028	0.009	0.021	0.012	−0.009	0.006	−0.052	0.009	−0.093	0.007
134.95	0.016	0.012	0.032	0.011	0.027	0.013	0.001	0.008	−0.041	0.011	−0.112	0.007
139.95	0.010	0.011	0.028	0.011	0.040	0.007	0.033	0.008	−0.020	0.012	−0.049	0.008
144.95	0.005	0.010	0.032	0.011	0.046	0.009	0.098	0.011	0.108	0.013	0.136	0.016
147.45	...	...	...	...	...	...	...	...	0.169	0.014	...	...
149.95	0.008	0.010[a]	0.027	0.011	0.063	0.014	0.151	0.010	0.204	0.013	0.281	0.010
154.95	0.010	0.011[a]	0.017	0.009	0.059	0.008	0.161	0.009	0.209	0.014	0.297	0.009

[a] Add 0.05° to c.m. scattering angle.
[b] Subtract 0.05° from c.m. scattering angle.

zation enhancement due to beam scraping is believed to contribute no more than 0.01 scale error, and tends to compensate for error due to (1). The error due to (3) is probably of order 0.005 (Ref. 14)—and also tends to reduce the effect of (1). Terminal depolarization reduces the vector polarization by no more than 0.001 (Ref. 22). Taking all these effects together, we feel that ± 0.02 times A_y is a reasonable estimate of the scale error in our A_y measurements.

At the larger scattering angles, multiple scattering of the detected particles in the gas cell exit foil may be significant. The problem is potentially most serious for the recoil ^{3}He particles, which have multiple-scattering angles on the order of 1.0°–2.5°. For the analyzing power, the measured value $\langle A_y(\theta_0)\rangle_\epsilon$ is related to the true value $A_y(\theta_0)$ by the formula

$$\langle A_y(\theta_0)\rangle_\epsilon = A_y(\theta_0) + \tfrac{1}{4}\epsilon^2\left[\cot\theta_0 A_y'(\theta_0) + \frac{2}{\sigma_0(\theta_0)}\sigma_0'(\theta_0)A_y'(\theta_0) + A_y''(\theta_0) - \csc^2\theta_0 A_y(\theta_0)\right]. \quad (4)$$

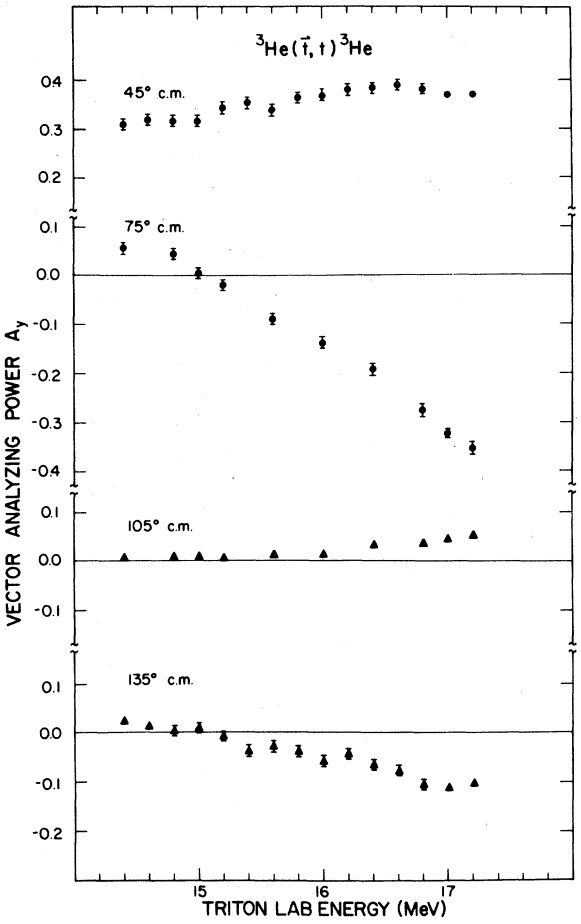

FIG. 6. Excitation functions of A_y for $^3\mathrm{He}+\vec{t}$ elastic scattering at c.m. angles of 45.05°, 75.10°, 104.90°, and 134.95°. Error bars shown are statistical only.

Here ϵ is the rms multiple scattering angle in radians,[23] θ_0 is the lab angle of interest, $\sigma_0(\theta_0)$ is the lab differential cross section, and the primes indicate differentiation with respect to the *lab* angle in radians. Although Eq. (4) was derived for solid targets, we have found that it gives reasonably accurate estimates for gas targets as well.

From Eq. (4), it is apparent that multiple-scattering corrections to A_y may be large on steep slopes in either σ_0 or A_y; in regions where A_y has a large curvature; or near maxima of A_y. The angular distribution data were checked numerically for significant multiple-scattering corrections at all angles where these effects might be important. In all cases, the corrections were found to be less than 0.001—which is significantly less than statistical errors. In addition, the 16-MeV angular distribution data, taken with the Kapton gas cell, agree with the 16-MeV excitation function data taken with the Havar gas target. Since ϵ for 2.5-μm Havar foil is approximately 3 times as large as ϵ for 6-μm Kapton, this demonstrates that multiple-scattering corrections to A_y are negligible in this experiment.

B. Differential cross section

The laboratory cross sections σ_0 were computed from the formula

$$\sigma_0(\theta_0) = \frac{Y \sin\theta_0}{nNG}, \tag{5}$$

where Y is the yield of scattered particles, θ_0 is the laboratory scattering angle, n is the number of beam particles, N the number of target particles

TABLE II. Analyzing power excitation functions $A_y(E)$ for $^3\mathrm{He}(\vec{t},t)^3\mathrm{He}$. The indicated errors ΔA_y are relative only. Scale error is ± 0.02 times A_y.

Triton lab energy	c.m. scattering angle (deg)							
	45.05		75.10		104.90		134.95	
(MeV)	A_y	ΔA_y	A_y	ΔA_y	A_y	ΔA_y	A_y	ΔA_y
14.42	0.310	0.010	0.057	0.010	0.008	0.006	0.025	0.010
14.62	0.318	0.010	...	...	...	...	0.014	0.006
14.82	0.317	0.010	0.045	0.010	0.009	0.006	0.004	0.010
15.02	0.317	0.010	0.007	0.006	0.009	0.006	0.009	0.010
15.22	0.343	0.010	−0.018	0.012	0.005	0.006	−0.006	0.009
15.42	0.354	0.011	...	...	...	...	−0.038	0.011
15.62	0.339	0.011	−0.088	0.012	0.011	0.006	−0.028	0.011
15.82	0.361	0.011	...	...	...	...	−0.038	0.011
16.02	0.367	0.011	−0.137	0.012	0.013	0.006	−0.057	0.011
16.22	0.378	0.010	...	...	...	...	−0.042	0.011
16.42	0.382	0.011	−0.191	0.013	0.031	0.006	−0.064	0.011
16.62	0.388	0.011	...	...	...	...	−0.077	0.011
16.82	0.380	0.011	−0.275	0.013	0.035	0.006	−0.106	0.011
17.02	0.367	0.008	−0.324	0.009	0.043	0.006	−0.112	0.008
17.22	0.368	0.008	−0.352	0.013	0.050	0.006	−0.102	0.008

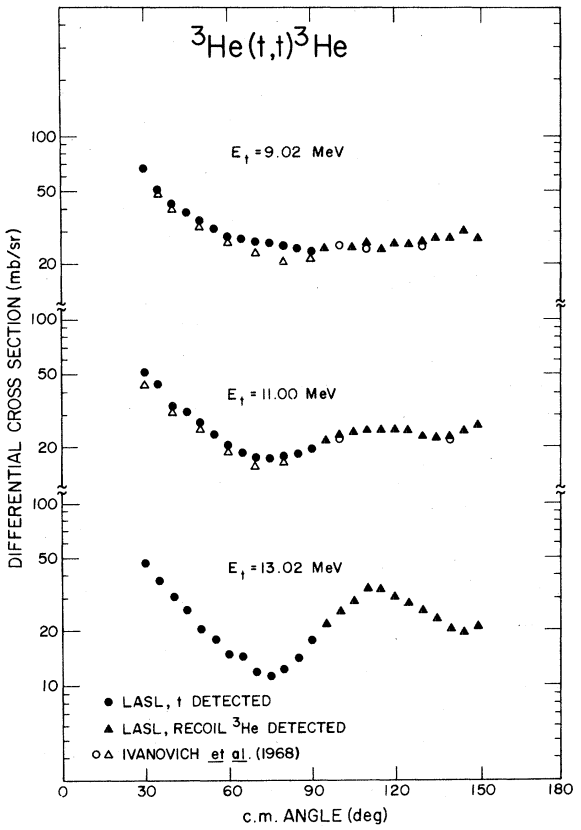

FIG. 7. Angular distributions of the c.m. differential cross section for ^{3}He+t elastic scattering at triton lab energies of 9.02, 11.00, and 13.02 MeV. Relative errors are smaller than the plotting symbols. The data shown as open circles and open triangles are from Ref. 9.

per unit volume, and G is the gas-target geometry factor.[13] For symmetric geometry, the yield is given by Eq. (2), and G is the geometric mean of the left- and right-detector geometry factors. In the calculations for this experiment, we found that G was adequately represented by the first-order term G_{00} in the expansion given by Silverstein.[13]

Since this experiment marked the first use of the Supercube scattering chamber to measure cross sections with a gas target, we made additional measurements at selected energies and angles using the LASL 75-cm-diam scattering chamber[24] and a Kapton gas cell. This chamber is equipped for high-precision cross section measurements (scale errors less than 1%) and incorporates target pressure and temperature monitors not available in the Supercube. A total of 31 points, at 9.02, 13.02, and 17.02 MeV, were measured in this way, and were found to agree with the Supercube data to within the stated accuracies.

The differential cross sections are shown in Figs. 7 and 8 and listed in Table III. Cross sections are not quoted for $\theta_{c.m.}$=25° or 155° (θ =12.5°), because it appeared that the detector snouts (see Fig. 1) were cutting into the beam leaving the gas target. This reduces the current reaching the Faraday cup and thus results in too large an apparent cross section.

The 16-MeV cross section agrees quite well with that reported at 15.89 MeV by Bacher, Spiger, and Tombrello,[8] except in the back-angle minimum. On the other hand, the forward-angle cross sections at 9 and 11 MeV are somewhat higher than those measured by Ivanovich, Young, and Ohlsen.[9] Since the measurements in the 75-cm scattering chamber confirm the values extracted from the Supercube measurements, there may be some systematic difficulty with the data of Ref. 9.

The relative errors in the cross-section data arise mainly from (1) uncertainties in reading the

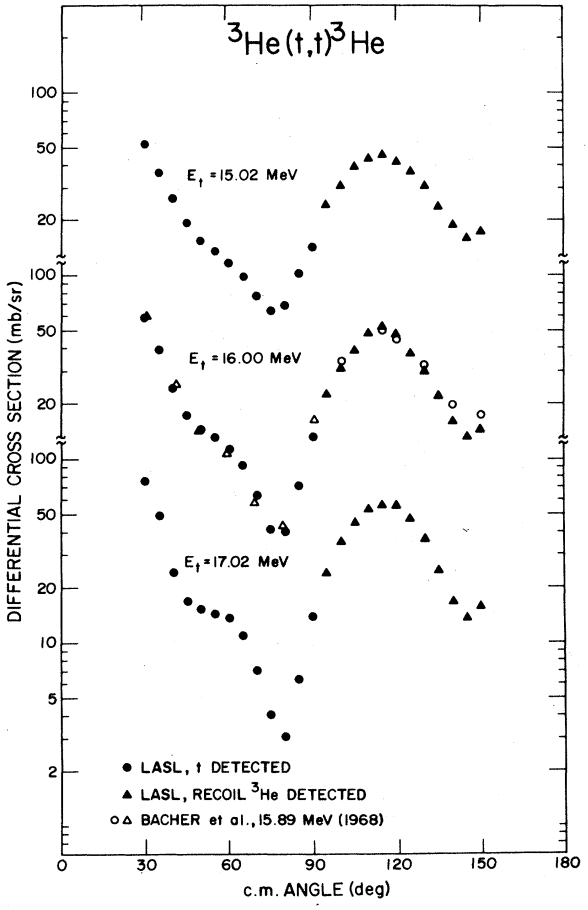

FIG. 8. Angular distributions of the c.m. differential cross section for ^{3}He+t elastic scattering at triton lab energies of 15.02, 16.00, and 17.02 MeV. Relative errors are smaller than the plotting symbols. The data shown as open circles and open triangles are from Ref. 8.

TABLE III. c.m. differential cross sections $\sigma(\theta)$ for $^3\mathrm{He}(t,t)^3\mathrm{He}$ at the stated energies, in mb/sr. Percent errors $\Delta\sigma$ are relative errors only. The scale error is 1.1%.

c.m. angle (deg)	Triton lab energy 9.02 MeV σ	9.02 MeV Δσ (%)	11.00 MeV σ	11.00 MeV Δσ(%)	13.02 MeV σ	13.02 MeV Δσ(%)	15.02 MeV σ	15.02 MeV Δσ (%)	16.00 (MeV) σ	16.00 (MeV) Δσ (%)	17.02 MeV σ	17.02 MeV Δσ (%)
30.05	65.8	2.0	50.7	2.0	46.1	0.7	51.8	2.0	59.0	2.1	76.4	2.2
35.05	51.4	2.0	44.7	2.0	37.7	0.7	36.5	2.0	39.5	2.1	48.2	2.1
40.05	43.6	0.8	33.7	3.6	30.2	0.8	25.9	2.0	24.7	2.0	24.0	2.1
45.05	38.4	0.9	31.0	2.0	25.1	0.9	19.4	2.0	17.2	2.1	16.8	2.0
50.05	34.7	1.0	27.8	2.0	20.1	2.0	15.5	2.0	14.2	2.1	15.0	2.0
55.05	31.0	2.0	23.7	2.1	17.1	2.0	13.5	2.0	13.0	2.2	14.4[a]	2.0
60.05	28.2	2.0	20.5	2.8	14.8	2.0	11.7	2.0	11.4[a]	2.2	13.6[a]	2.0
65.05	27.5	2.0	18.8	2.5	14.4	2.0	9.7[a]	2.0	9.3[a]	2.1	10.8[a]	2.0
70.05	26.5	2.0	17.7	2.2	11.8	1.1	7.8[a]	2.0	6.4[a]	2.2	7.1[a]	2.0
75.05	26.1	2.0	17.2	2.1	11.2	1.2	6.5[a]	2.0	4.2[a]	2.4	4.1[a]	2.0
80.05	25.0	5.0	17.9	2.0	12.0	2.0	7.0[a]	2.1	4.1[a]	2.4	3.1[a]	2.0
85.05	24.6	1.0	18.3	2.1	14.0[a]	1.2	10.2[a]	2.0	7.3[a]	2.3	6.4[a]	2.0
90.05	23.4	1.0	19.5	2.2	17.5[a]	1.1	14.1[a]	2.3	13.1[a]	2.4	13.8[a]	2.1
94.95	24.8	1.1	22.1	2.1	23.8	1.2	24.5[b]	3.1	22.9[b]	2.3	24.1[b]	2.1
99.95	...	...	23.9	2.1	25.7	1.2	30.8[b]	2.0	31.0[b]	2.1	36.3[b]	2.1
104.95	25.1	2.0	24.4	2.1	28.9	1.0	39.8	2.0	39.7[b]	2.0	46.3[b]	2.0
109.95	26.1	2.0	25.6	2.2	31.8	1.0	43.7	2.0	44.5[b]	2.0	53.1[b]	2.0
114.95	24.6	2.0	25.5	2.5	34.6	2.0	44.4	2.0	46.7	2.0	56.5[b]	2.0
119.95	26.2	2.0	25.3	2.8	31.0	2.0	42.0	2.0	44.0	2.0	56.6	2.0
124.95	25.1	2.0	25.2	2.1	28.6	2.0	37.0	2.0	38.4	2.0	47.8	2.1
129.95	27.7	1.0	23.6	2.1	26.0	2.0	31.4	2.0	30.2	2.0	35.0	2.3
134.95	28.0	1.0	22.9	2.1	23.1	0.9	23.9	2.0	22.4	2.1	25.4	2.1
139.95	29.3	0.9	22.9	3.6	20.2	0.9	18.9	2.0	16.1	2.1	17.2	2.5
144.95	29.9	2.0	24.9	2.2	19.5	0.9	16.1	2.1	13.3	2.1	13.9	3.2
149.95	28.3[a]	2.0	26.7	2.1	21.3	0.9	17.5	2.1	14.8	2.1	16.1	2.0

[a] Add 0.05° to c.m. scattering angle.
[b] Subtract 0.05° from c.m. scattering angle.

target gas pressure from the Wallace-Tiernan gauge, (2) statistical errors in the number of counts, (3) errors in the setting of peak and background gates, (4) random pressure and temperature fluctuations in the target, (5) beam-current integration, and (6) beam-position instability and/or detector-position uncertainty. The dominant factor in the relative error is (1), which is estimated to be 1.7%. This corresponds to an error of ±5 Torr in reading the pressure gauge attached to the gas target. The total error due to (3), (4), (5), and (6) is estimated to be 1.0%, based on previous LASL experiments with similar targets[24] and on the geometry of the Supercube scattering chamber. When statistical errors due to (2) are included, the overall relative error is 2.5% or less for almost all the data.

The scale errors for the cross section may be traced to (1) calibration error in the pressure gauge, (2) calibration error in the current integrator, (3) purity of the target gas, and (4) uncertainty in the geometry factor G [Eq. (5)]. The error due to (1) is 1.0%, while that due to (2) is of order 0.2%.[24] The purity of the ^{3}He target gas was determined to be 99.5% ± 0.3% by measuring the relative elastic-scattering yields from ^{3}He and the principal contaminants (air and ^{3}He) in the target gas. Finally, the slits used in the experiments were measured with a Leitz split-image optical comparator, from which measurements the G factor is estimated to be known to ±0.2%. The first-order correction to G [Ref. 13, Eq. (5c.1)] is 0.07%, so deviations of G from G_{00} are of no consequence. The over-all scale error which we assign to our data is, therefore, 1.1%.

At the higher energies, the sharpness of the forward- and back-angle minima and the steep slopes in the angular distributions suggest a possible need for multiple-scattering corrections. We used the solid-target multiple-scattering formula[25]

$$\langle\sigma_0(\theta_0)\rangle_\epsilon = \sigma_0(\theta_0) + \tfrac{1}{4}\epsilon^2[\cot\theta_0\sigma_0'(\theta_0) + \sigma_0''(\theta_0)] \qquad (6)$$

to make these corrections. [The symbols em-

ployed in Eq. (6) have the same meaning as those in Eq. (4).] We found that the correction due to the first-derivative term was negligible, but that the second-derivative term contributed a −2.6% correction at the back-angle minimum, for the 17-MeV data. Corrections of smaller magnitude were required at the minima in the 15- and 16-MeV angular distributions.

For both analyzing power and cross section, the ±0.02° uncertainty in the detector position may contribute significantly to the relative error in regions where the angular distribution has a steep slope. Calculations with the present data showed this effect to be negligible for all of the analyzing power angular distributions. For a few cross section data points, however, this angular uncertainty increased the relative error by 0.1—0.2%. The relative errors in Table III include this effect where it is important.

IV. DISCUSSION AND CONCLUSIONS

This paper presents the first available analyzing-power measurements for ^{3}He + $\vec{t}$ elastic scattering, and adds to the already extensive store of ^{3}He + t cross sections.[8,9,26] These data, coupled with the recent ^{3}H+$^3\vec{\text{He}}$ analyzing power measurements made at the University of Birmingham[27] will be of significant value for studies of the ^{6}Li system. In particular, the dramatic change in the shape of the analyzing-power angular distributions above 15 MeV suggests strong effects from the ^{6}Li resonances at 25.0 and 26.6 MeV.[1] The well-known sensitivity of A_y to the phases of terms in the complex scattering matrix means that these changes in shape should help to determine those terms with less ambiguity than is possible from cross sections alone.

The analysis of these data poses some difficult problems. The resonating group calculations by Thompson and Tang,[2] and the phase-shift analyses by Bacher *et al.*[8] and Batten *et al.*[26] were done in the single channel approximation, with l-dependent phase shifts only. As Thompson and Tang have pointed out, this approximation is clearly inadequate, because of the strength of the ^{3}He-$(t,d)^4$He reaction channel. Moreover, unsplit phases cannot be used to fit analyzing power data. The resonating group calculation of Ref. 3 incorporates an absorptive central potential and gives channel-spin-dependent complex phases, but it also predicts zero analyzing power, since it does not take account of spin-dependent nucleon-nucleon forces.

We attempted an analysis of the present data using a modified version of the code CPHASE,[28] which fits cross sections and analyzing powers for spin-$\frac{1}{2}$ on spin-$\frac{1}{2}$ elastic scattering. The program uses complex S- and J-dependent phases for $l = 0, 1, \ldots, 5$, with real triplet-singlet mixing parameters in the p, d, and f waves to simulate the off-diagonal terms of the scattering matrix. The cross-section and analyzing power angular distributions are fitted simultaneously at a single energy by a gradient-search routine.

With the exception of the 17-MeV data, good fits could be obtained at each energy, with χ^2 on the order of 1.5 per point. However, the solutions we found could not be extended smoothly to neighboring energies, even though the differences between parameters at different energies were generally small (on the order of 5 to 10°). For complex phase shifts through $l = 5$, in fact, the number of variable parameters nearly equals the number of data points in the angular distributions —so that the fitting problem is close to being mathematically overdetermined. In addition, there were no physical constraints (e.g., the exclusion principle[3]) on any of the phases in our calculations.

We believe, therefore, that an energy-dependent analysis—in the spirit of the recent work on $p + {}^4$He scattering by Dodder *et al.*[29]—is the most appropriate way to obtain a physically-meaningful phenomenological fit to the present data. Since measurements are now available for cross sections[30] and analyzing powers[31] for the ^{3}He($\vec{t}$, d)^{4}He reaction in the appropriate energy range, these could also be incorporated into the calculation to take proper account of the major competing reaction channel. We are currently working on such an analysis using the energy-dependent R-matrix code of Dodder and Hale.[29,32]

It is a pleasure to thank Mr. Louis Morrison for his assistance in operating and maintaining the polarized triton source, and the staff of the LASL tandem Van de Graaff facility for their support in the operation of the accelerator.

---

*Visiting Staff Member from the University of Minnesota.

† Visiting Staff Member from the Eidgenossische Technische Hochschule, Zurich, Switzerland.

‡Work supported by the U. S. ERDA.

[1]For a summary of available data, see F. Ajzenberg-Selove and T. Lauritsen, Nucl. Phys. A227, 1 (1974).

[2]D. R. Thompson and Y. C. Tang, Nucl. Phys. A106, 591 (1968).

[3]R. E. Brown, F. S. Chwieroth, Y. C. Tang, and D. R. Thompson, Nucl. Phys. A230, 189 (1974).

[4]H. H. Hackenbroich, P. Heiss, and Le-Chi-Niem, Nucl.

Phys. A221, 461 (1974).
[5]W. Grüebler, P. A. Schmelzbach, V. König, R. Risler, and D. Boerma, Nucl. Phys. A242, 265 (1975), and references therein.
[6]W. E. Burcham, O. Karban, S. Oh, and W. B. Powell, Nucl. Instrum. Methods 116, 1 (1974).
[7]R. A. Hardekopf, G. G. Ohlsen, R. V. Poore, and N. Jarmie, Phys. Rev. C 13, 2127 (1976).
[8]A. D. Bacher, R. J. Spiger, and T. A. Tombrello, Nucl. Phys. A119, 481 (1968).
[9]M. Ivanovich, P. G. Young, and G. G. Ohlsen, Nucl. Phys. A110, 441 (1968).
[10]Havar is a cobalt "super-alloy" manufactured by Hamilton Technology, Inc., Lancaster, Pennsylvania. Kapton is a polyimide film made by duPont, Inc., Wilmington, Delaware.
[11]P. A. Lovoi, Ph.D. dissertation, 1975 (unpublished), available as Los Alamos Scientific Laboratory Report No. LA-6041-T (unpublished).
[12]G. G. Ohlsen and P. A. Lovoi, in *Proceedings of the Fourth International Symposium on Polarization Phenomena in Nuclear Reactions*, edited by W. Grüebler and V. König (Birkhäuser, Basel, 1976).
[13]E. A. Silverstein, Nucl. Instrum. Methods. 4, 53 (1959).
[14]G. G. Ohlsen, J. L. McKibben, G. P. Lawrence, P. W. Keaton, Jr., and D. D. Armstrong, Phys. Rev. Lett. 27, 599 (1971).
[15]D. D. Armstrong, J. G. Beery, E. R. Flynn, W. S. Hall, P. W. Keaton, Jr., and M. P. Kellogg, Nucl. Instrum. Methods. 70, 69 (1969).
[16]The definitions of "up" and "down" for the quantization axis of the beam, and of "left" and "right" for the detectors, follow the Basel convention.
[17]G. G. Ohlsen and P. W. Keaton, Jr., Nucl. Instrum. Methods. 109, 41 (1973).
[18]E. Huenges, H. Rösler, and H. Vonach, Phys. Lett. 46B, 361 (1973).
[19]R. G. Clarkson and N. Jarmie, Comput. Phys. Commun. 2, 433 (1971).
[20]N. Bohr, Phil. Mag. 30, 581 (1915). See also H. A. Bethe and J. Ashkin, in *Experimental Nuclear Physics*, edited by E. Segrè (Wiley, New York, 1953), Vol. I., p. 243.
[21]G. G. Ohlsen, P. A. Lovoi, G. C. Salzman, U. Meyer-Berkhout, C. K. Mitchell, and W. Grüebler, Phys. Rev. C 8, 1262 (1973).
[22]G. G. Ohlsen, P. A. Lovoi, R. A. Hardekopf, R. L. Walter, and P. W. Lisowski, Nucl. Instrum. Methods. 131, 489 (1975).
[23]J. B. Marion and B. A. Zimmerman, Nucl. Instrum. Methods. 51, 93 (1967).
[24]N. Jarmie, J. H. Jett, J. L. Detch, Jr., and R. L. Hutson, Phys. Rev. C 3, 10 (1971).
[25]C. T. Chase and R. T. Cox, Phys. Rev. 58, 243 (1940).
[26]R. J. Batten, D. L. Clough, J. B. A. England, R. G. Harris, and D. H. Worledge, Nucl. Phys. A151, 56 (1970).
[27]J. B. A. England and R. Vlastou (private communication).
[28]R. A. Hardekopf, P. W. Lisowski, T. C. Rhea, R. L. Walter, and T. B. Clegg, Nucl. Phys. A191, 481 (1972).
[29]D. C. Dodder, G. M. Hale, Nelson Jarmie, J. H. Jett, P. W. Keaton, Jr., R. A. Nisley, and K. Witte, Phys. Rev. C 15, 518 (1977).
[30]W. J. Roberts, E. E. Gross, and E. Newman, Phys. Rev. C 9, 149 (1974), and references therein.
[31]R. F. Haglund, Jr., G. G. Ohlsen, R. A. Hardekopf, R. E. Brown, and N. Jarmie, Bull. Am. Phys. Soc. 21, 533 (1976); (unpublished).
[32]D. C. Dodder, in *Proceedings of the Fourth International Symposium on Polarization Phenomena in Nuclear Reactions* (see Ref. 12), p. 167.